An update to this article is included at the end

Cancer Cell
Article

Molecular Mechanism of SSR128129E, an Extracellularly Acting, Small-Molecule, Allosteric Inhibitor of FGF Receptor Signaling

Corentin Herbert,[1,11] Ulrich Schieborr,[2,11] Krishna Saxena,[2,11] Jarek Juraszek,[3,11] Frederik De Smet,[4,5,11] Chantal Alcouffe,[1] Marc Bianciotto,[1] Giorgio Saladino,[3] David Sibrac,[1] Denis Kudlinzki,[2] Sridhar Sreeramulu,[2] Alan Brown,[7] Patrice Rigon,[1] Jean-Pascal Herault,[1] Gilbert Lassalle,[1] Tom L. Blundell,[7] Frederic Rousseau,[8] Ann Gils,[6] Joost Schymkowitz,[8] Peter Tompa,[9,10] Jean-Marc Herbert,[1] Peter Carmeliet,[4,5,11] Francesco Luigi Gervasio,[3,11,*] Harald Schwalbe,[2,11,*] and Françoise Bono[1,11,*]

[1]E2C and LGCR-SDI Department, Sanofi Research and Development, 31100 Toulouse, France
[2]Institute for Organic Chemistry and Chemical Biology, Center for Biomolecular Magnetic Resonance (BMRZ), University of Frankfurt, D-60438 Frankfurt, Germany
[3]Computational Biophysics Group, Spanish National Cancer Research Center (CNIO), E-28029 Madrid, Spain
[4]Laboratory of Angiogenesis and Neurovascular Link, Vesalius Research Center (VRC), VIB, 3000 Leuven, Belgium
[5]Laboratory of Angiogenesis and Neurovascular Link, Vesalius Research Center (VRC)
[6]Laboratory for Pharmaceutical Biology, Pharmaceutical Sciences
KU Leuven, 3000 Leuven, Belgium
[7]Department of Biochemistry, University of Cambridge, CB2 1GA Cambridge, UK
[8]VIB Switch Laboratory, Department of Cellular and Molecular Medicine, VIB-KU Leuven, 3000 Leuven, Belgium
[9]VIB Department of Structural Biology, Vrije Universiteit Brussel, 1050 Brussels, Belgium
[10]Institute of Enzymology, Research Center for Natural Sciences, Hungarian Academy of Sciences, H-1113 Budapest, Hungary
[11]These authors contributed equally to this work
*Correspondence: flgervasio@cnio.es (F.L.G.), schwalbe@nmr.uni-frankfurt.de (H.S.), francoise.bono@sanofi-aventis.com (F.B.)
http://dx.doi.org/10.1016/j.ccr.2013.02.018

SUMMARY

The fibroblast growth factor (FGF)/fibroblast growth factor receptor (FGFR) signaling network plays an important role in cell growth, survival, differentiation, and angiogenesis. Deregulation of FGFR signaling can lead to cancer development. Here, we report an FGFR inhibitor, SSR128129E (SSR), that binds to the extracellular part of the receptor. SSR does not compete with FGF for binding to FGFR but inhibits FGF-induced signaling linked to FGFR internalization in an allosteric manner, as shown by crystallography studies, nuclear magnetic resonance, Fourier transform infrared spectroscopy, molecular dynamics simulations, free energy calculations, structure-activity relationship analysis, and FGFR mutagenesis. Overall, SSR is a small molecule allosteric inhibitor of FGF/FGFR signaling, acting via binding to the extracellular part of the FGFR.

INTRODUCTION

Receptor tyrosine kinases (RTKs) constitute a major class of drug targets (Overington et al., 2006). Most efforts have been invested in developing agents that orthosterically compete for binding between RTKs with their endogenous ligands, such as antibodies recognizing growth factors or their receptors or small molecules that inhibit their tyrosine kinase (TK) activity (Gasparini et al., 2005; Zhang et al., 2009). Only a few drugs that interact with allosteric sites have been developed for ion channels and G protein-coupled receptors (Christopoulos, 2002; Conn et al., 2009) and kinases (Zhang et al., 2009). In contrast to orthosteric inhibitors, advantages of allosteric drugs include specificity and safety (Christopoulos, 2002).

Significance

FGF receptors (FGFRs) belong to the receptor tyrosine kinase (RTK) superfamily, which is of immense importance for numerous (patho-)physiological processes and a key target for drug development. Most drugs targeting the extracellular domains of RTKs are traditionally antibodies, but small chemical compounds, acting extracellularly, which are capable of inhibiting RTK signaling, have not been described yet. This study identified an extracellularly binding allosteric inhibitor of FGFRs and investigated its allosteric mechanisms. Besides therapeutic advantages of allosteric drugs, our data warrant further development of additional small, extracellularly acting, allosteric molecules for targeting this important class of receptors.

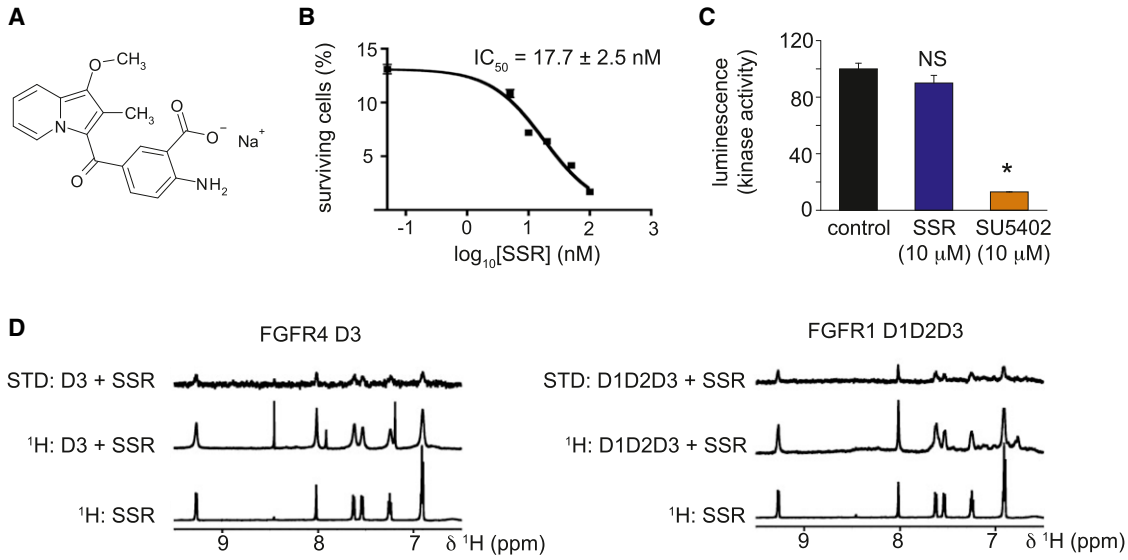

Figure 1. Chemical Structure, Cellular Effects, and NMR of SSR

(A) Chemical structure of SSR128129E (SSR).

(B) Apoptosis assay to study SSR's potency of inhibiting EC survival (mean ± SEM; n = 3).

(C) FGFR2-kinase assay to compare the effect of SSR and SU5402 (mean ± SEM; n = 3). The asterisk indicates that $p < 0.05$. NS, not significant.

(D) ^{1}H and STD-NMR spectra of SSR in the presence of FGFR1 and FGFR4 as compared to the ^{1}H-NMR spectrum of SSR alone.

See also Figure S1 and Table S1.

By using a high-throughput scintillation proximity binding assay (SPA), we identified compounds that inhibited binding of ^{125}I-FGF2 to the extracellular domain of FGFR1, comprising three immunoglobulin-like domains D1–D3 coupled to an Fc-fragment (FGFR1-D1D2D3/Fc). After screening $>10^5$ compounds and chemical optimization, one compound (SSR128129E, abbreviated as "SSR") inhibited ^{125}I-FGF2 binding with μM affinity, although this effect was not saturated (Bono et al., 2013). These findings suggested a modulation in fibroblast growth factor (FGF) binding but not necessarily binding competition. Further, SSR reduced FGFR phosphorylation but did not cross the plasma membrane, while inhibiting cell proliferation at nM potency. The discrepancy of the inhibition constants between the SPA results and proliferation assay led us to investigate the molecular mechanisms of SSR. Pharmacological experiments showed that this compound inhibited FGF receptor (FGFR) signaling via an allosteric mechanism (Bono et al., 2013), which we studied in more molecular detail here.

RESULTS

SSR128129E Inhibits FGFR and Binds to Its Extracellular Domain

We identified SSR128129E, referred to as "SSR" (Figure 1A), which inhibited the binding of ^{125}I-FGF2 to the extracellular domain (ECD) of FGFR1 at μM concentrations in a SPA assay (Bono et al., 2013). SSR dose-dependently inhibited the survival of endothelial cells (ECs) ($IC_{50} < 30$ nM; Figure 1B).

Since SSR's effects on FGFR signaling did not result from an inhibition of FGF binding to FGFRs (Bono et al., 2013), impaired dimerization of FGFRs or FGF ligands (Figures S1A and S1B available online), or TK inhibition (Figure 1C), we used saturation transfer difference (STD)-nuclear magnetic resonance (NMR) to analyze if, after FGFR irradiation, the NMR signal (saturation) would spread to SSR, which would indicate that SSR interacts with FGF. However, SSR did not bind FGF1 or FGF2 (Figure S1C).

We assessed if SSR bound FGFR-ECD, in which D2 and D3 constitute the major binding site for FGFs and coreceptors. STD-NMR showed that SSR bound all constructs containing D2 and/or D3 (Table S1). Figure 1D shows the STD-NMR spectra of FGFR1 and FGFR4 with SSR. Together with the functional assays, these data suggest a direct (orthosteric) or indirect (allosteric) inhibition of FGF binding to ECD of FGFR and/or the biological function of the receptor.

SSR Inhibits FGF-Induced Signaling and Endocytosis Pathways

To dissect how SSR interfered with FGFR, we studied its effect on ERK1/2 activation and FGFR endocytosis. SSR blocked the FGF2-induced increase in ERK1/2 phosphorylation (Figure 2A) and translocation of cell surface FGFR4 to the cytosol (Figure 2B). In addition, SSR inhibited the FGF2-induced intracellular accumulation of early endosomal antigen1 positive ($EEA1^+$) vesicles, the destination of internalized FGFRs (Figures 2C and 2D). Similar effects of SSR on FGFR internalization and phosphorylation of FRS-2 (target of FGFR2) and ERK1/2 were observed in human gastric SNU-16 cancer cells, in which these processes rely on FGF7/FGFR2 (Figures 2E and 2F), and in FGFR2-overexpressing L6 cells (see below). Blockage of FGFR internalization could explain the inhibition of FGFR signaling, though other opinions exist (Belleudi et al., 2007; Reilly et al., 2004).

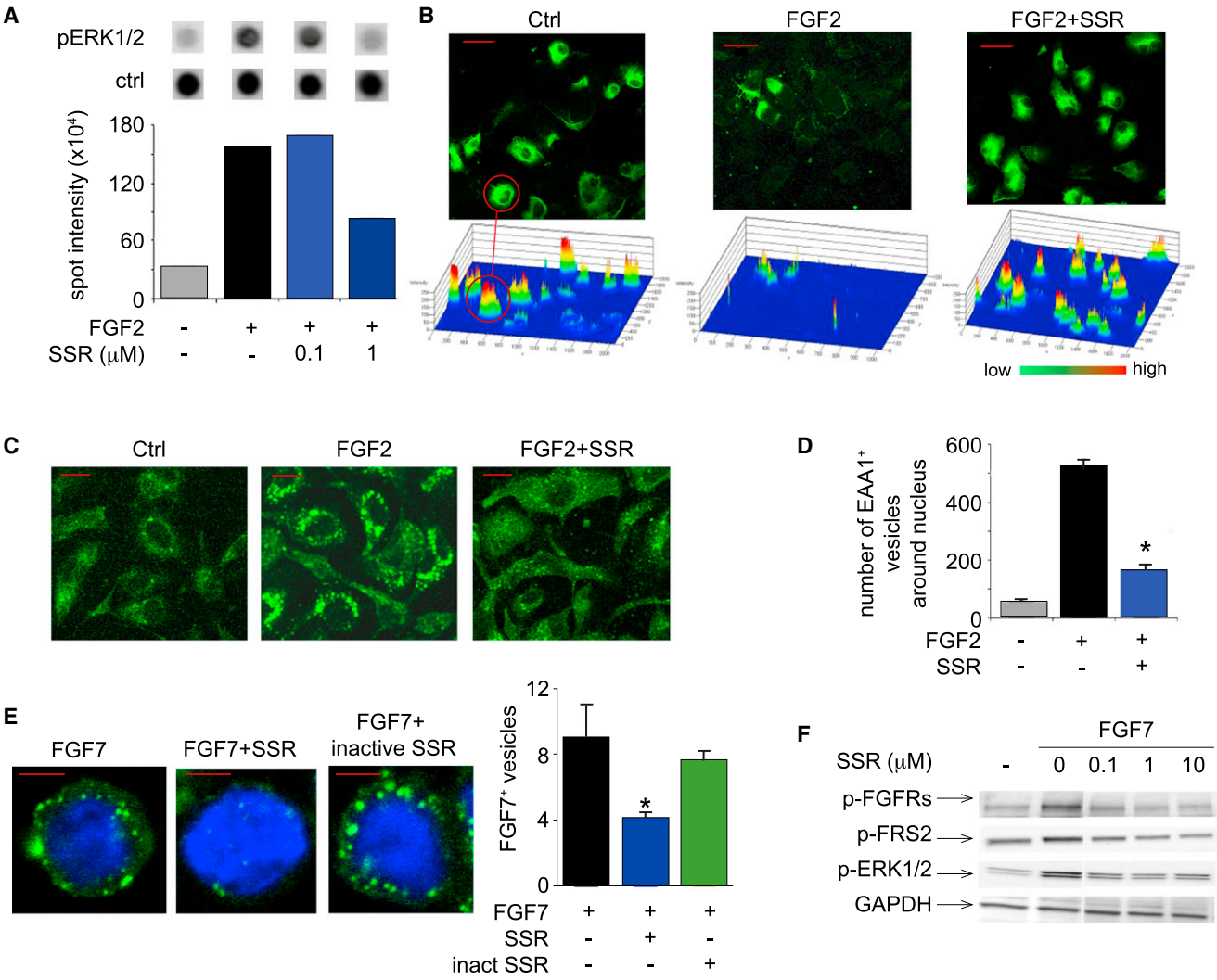

Figure 2. Effect of SSR on FGFR-Signaling and Endocytosis

(A) Phosphoproteome profiler array of ECs in baseline and response to FGF2 in the presence or absence of SSR (n = 3).

(B) Micrographs of cell surface-localized FGFR to study FGF2-induced internalization of FGFR4 with or without SSR (top). Immunoreactive signal for single cells is quantified in the 2.5D intensity plot (bottom).

(C and D) Staining of FGF2-stimulated ECs for EEA1 in the presence or absence of SSR. Representative images are shown in (C) and quantification result of EEA1$^+$ vesicles is shown in (D, n = 3).

(E) Stimulation of SNU-16 cells with FGF7-alexa488 to study SSR's effect on endosomal trafficking; SSR119501: inactive SSR-analog (n = 3).

(F) Immunoblotting of SNU-16 cell extracts to study the effect of SSR on FGF7-induced phosphorylation of FGFR2 (p-FGFR), FRS-2 (p-FRS-2), and ERK1/2 (p-ERK1/2). GAPDH: loading control. Scale bars: 50 μm (B); 20 μm (C); 10 μm (E). In (D) and (E): mean ± SEM. The asterisk indicates $p < 0.05$.

Structural Properties of Extracellular FGFR Domains D2 and D3

To map the interaction site of SSR with FGFR-ECD, we first generated two-dimensional (2D) ^{15}N-HSQC NMR spectra of FGFR-ECD in the absence of SSR to obtain the protein's fingerprint. Peaks in this spectrum correspond to amide groups (and nitrogen-containing side-chains). Since chemical shift perturbations (CSPs) of these peaks are sensitive to the chemical environment, this technique allows identification of SSR interaction sites with FGFR-ECD.

The spectrum of D2 showed sharp peaks and spectral dispersion, as expected for a well-folded domain with defined structure, and all NMR resonances were assigned to a particular residue. In contrast, the signals of D3 could not be detected, because they were broadened beyond detection, indicating that D3 does not adopt a stable, persistent three-dimensional (3D)-fold (Figures S2A–S2F). This behavior is consistent with a transiently unfolded flexible state, a phenomenon confirmed by D3's high tendency to aggregate (data not shown). Because this behavior can be an inherent property of the domain or, alternatively, a preparation artifact compromising the analysis of a potential interaction with SSR, we generated preparations of functional, structured D3. However, optimization of conditions to solubilize D3, variations of D3 constructs (with/without

membrane or D2D3-Linker), or attachment of solubilizing fusion constructs (thioredoxin, protein G) all failed to yield spectra consistent with a stable D3 fold, while the other domains remained readily detectable (Figures S2A–S2D).

Such a very flexible (intrinsically disordered; Tompa, 2011) state of proteins can be characterized by computer simulations that estimate the preferred conformational state and stability of various parts of the protein. We therefore performed multi-μs-long, unbiased, all-atom, explicit-solvent molecular dynamics (MD) computer simulations with the Amber99SB*-ILDN force field. In line with NMR data, D3 was marginally stable and partially disordered in solution. The Thr^{319}-Arg^{330} region, which has an extended β-conformation in the crystal structure, tended to adopt an α-helical conformation and to detach from the protein core, leading to partial unfolding of the domain. Plasticity of this region, in particular of the βC′-βE loop (Pro^{307}-Val^{332}) plays a key role in the specificity of FGF binding to FGFR splice variants (Beenken and Mohammadi, 2009). Noteworthy, the algorithm AGADIR also predicted a propensity for α helix conformation of the Thr^{319}-Arg^{330} region, thus independently confirming the MD computer simulations.

To assess if the flexibility of D3 corresponds to a completely random (random coil) or compact but unfolded (molten globule [MG]) state and to verify the chemical purity and quality of the protein used in the NMR experiments, we performed FGFR2-D2D3 crystallization trials. We resolved a similar structure of the FGFR2-FGF1 complex, as reported (Plotnikov et al., 1999; Schlessinger et al., 2000). A defined electron density of D3 revealed a stable structure, suggesting that D3 is only marginally unstable and ready to fold in conditions of crystallization and/or upon forces taking place in the crystal. These observations are compatible with a molten globule state of D3 (in line with the increased aggregation propensity and disappearance of NMR peaks). Control experiments showed that the amino acid composition of the urea-unfolded D2D3 polypeptide chain was correct (Figures S2E and S2F), that D3 folding was not enforced by crystallization conditions (Figures S2G and S2H), and that D2D3 interacted with FGF1 (Figures S2G and S2I). Since the crystal structure indicates that D2 and D3 are needed to interact with FGF (Plotnikov et al., 1999; Schlessinger et al., 2000), these findings show that D3 is present and functional. Thus, D2 is well folded, while D3 is in an unfolded MG state that is ready to fold.

Mode of Action of SSR: Effects on D2

We then explored to which sites SSR binds in the FGFR ECD and used 2D NMR to determine the CSP values upon addition of SSR to D2 of FGFR1, FGFR2, and FGFR4. SSR-induced CSPs were mapped on the X-ray structure of FGF2/FGFR1-D2D3/heparin (Protein Data Bank [PDB] code 1FQ9; Schlessinger et al., 2000). The CSPs suggested a conserved binding site of SSR in the vicinity of—but not overlapping with—the heparin binding site of D2 (red balls show residues interacting with SSR in D2 of FGFRs; Figures 3A and 3B). Chemical shift titration analysis yielded a binding affinity of SSR to D2 of FGFR1, −2 and −4 in the mM range (Table S2). These affinities are two to three orders of magnitude too low to explain the μM SPA data. Moreover, the computational estimation of the free binding energy of SSR to FGFR2-D2 (~5 kcal/mol) is in line with the mM range of the observed K_D values (Figure 3C). Thus, an interaction of SSR with D2 alone cannot account for the cellular effects.

We therefore performed binding experiments with FGF/FGFR complexes. Since NMR signals only appear if the protein is labeled with ^{15}N isotope, FGFR or FGF was labeled separately to dissect to which component SSR binds. The effect of SSR on the 2D NMR spectra of (^{15}N)FGFR2-D2D3/FGF1 and FGFR1-D1D2D3/(^{15}N)FGF2 is shown in Figure 3D and mapped on the crystal structure 1FQ9 in Figure 3E. The spatial CSP clustering indicates a binding site for SSR at the interface between D2 and FGF, in agreement with the binding of SSR to D2 alone. Confirming STD-NMR experiments that SSR does not bind to FGF1 or FGF2, SSR induced CSPs in FGF only when a FGF/FGFR complex was formed. When analyzing the complex between FGFR1-D1D2D3 and (^{15}N)FGF2, two additional CSPs were observed: Asn^{101} (facing D2 in crystal structure 1FQ9) and Ala^{57} (facing D3; black circle in Figure 3E, bottom), suggesting an additional binding site for SSR in D3. To evaluate SSR's affinity for FGFR/FGF, we performed NMR titration experiments of FGF1/FGFR1-D1D2D3 with SSR, yielding an affinity constant in the low μM range (~50 μM; Figure 3F). Due to the structural disorder of D3, a binding mode could not be deduced. Together, the CSP data indicate a binding site on the interface between FGF and D2 and a potential binding site on D3. A role for D3 in SSR binding is supported by the mM affinity of SSR to D2 alone, too low to explain the biological effect.

Mode of Action of SSR: Low Resolution FGF-FGFR Crystals

To further assess the molecular basis of the allosteric interaction, we performed X-ray crystallography. Crystals of FGF1/FGFR2-D2D3 complexes with SSR could not be optimized to a suitable diffraction quality, but it was possible to generate crystals with SR128545 (abbreviated as "SR"; Figure S3A), a SSR analog with comparable cellular activity (Figure S3B). Limited by a diffraction resolution of 4.2 Å, the exact binding position of SR could not be visualized, but conformational protein backbone changes induced by the interaction with SR were detectable. Molecular replacement (MR) statistics of Phaser (McCoy et al., 2007) were used to compare the observed X-ray diffraction pattern to existing 3D models. This revealed single solutions without structural clashes when independently using the three separate domains (FGF1, FGFR2-D2, and FGFR2-D3) of the FGF1/FGFR2/heparin crystal structure (PDB code 1E0O; Pellegrini et al., 2000). These results confirm that the obtained crystal structures were in agreement with published results (PDB codes 1CVS and 1DJS). We also analyzed the translation function Z-scores (TFZ), as they are a measure of how well the MR model fits to X-ray data (a high score indicates a good match). TFZ scores in the presence of SR were smaller for D3 than for D2 or FGF1 (FGF1/SR = 23.1, FGFR2-D2/SR = 15.7, and FGFR2-D3/SR = 7.5), showing that the structure solution cannot explain the entire scattering pattern in the presence of SR but rather suggests a structural change induced by SR.

To confirm the above findings and to determine conformational dynamics, we refined the structure of the FGFR2-D2D3/FGF1/heparin/SR complex by generating polyalanine models using Refmac5 to obtain a model that best explains the experimental data (Murshudov et al., 1996). The electron density of

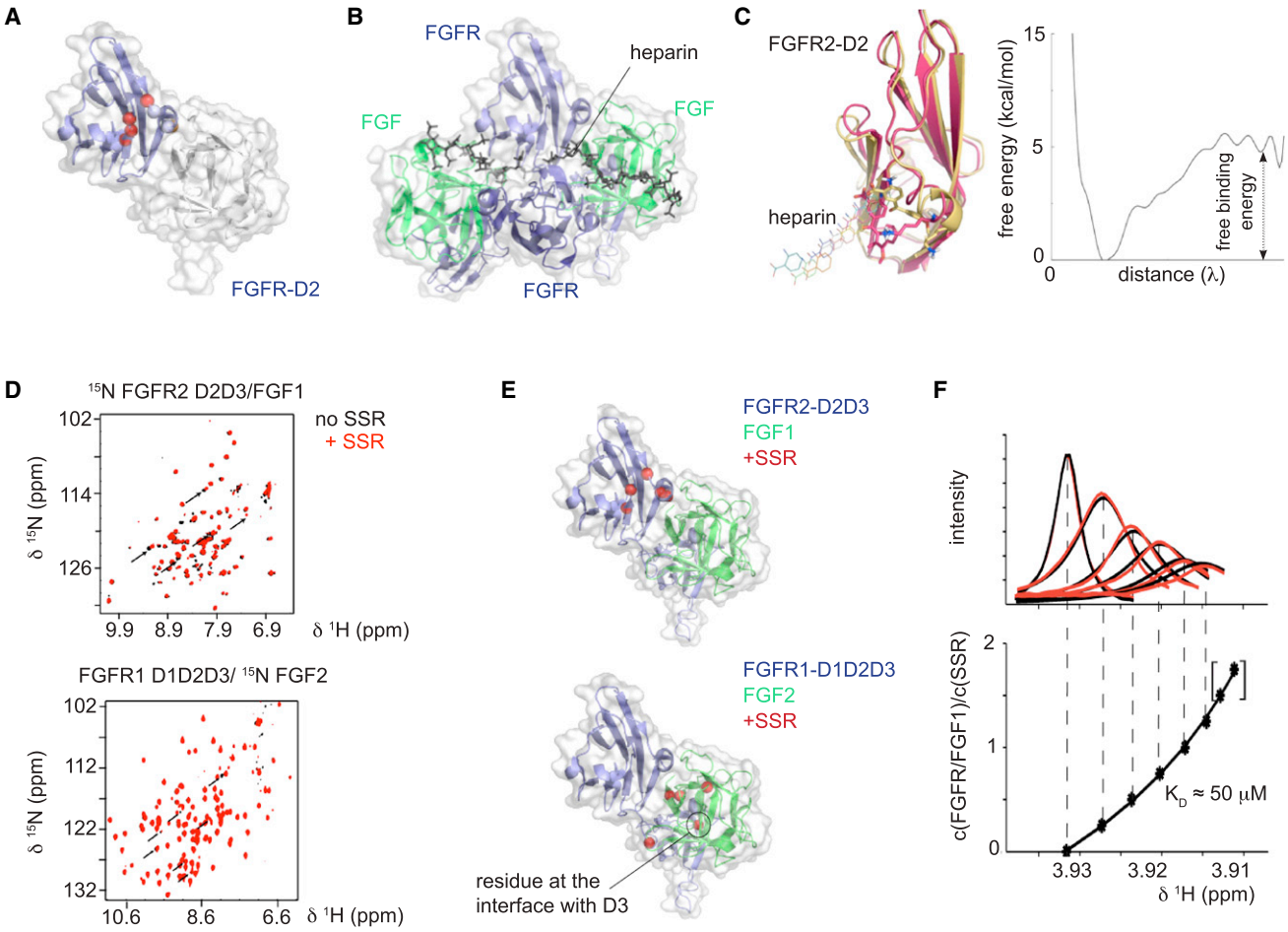

Figure 3. 2D-NMR Analysis and Free Energy Profiles

(A and B) Surface representation of FGFR (blue) and FGF (green), showing the SSR binding site in FGFR2 and FGFR4. Amide signals, shifting due to addition of SSR in 2D ^{15}N-HSQC NMR, were mapped onto the X-ray structure of FGFR1-D2D3/FGF2/heparin mimetic (1FQ9). (A) Highlight of the shifting amide residues of D2 of FGFR2 and FGFR4, induced by SSR. Red balls indicate residues shifting in both FGFRs (Thr^{150}, Phe^{170}, Arg^{171}, and Cys^{172}; numbering according to FGFR4). His^{151} and Arg^{154} (light blue balls) only shift in FGFR4-D2, and Lys^{164} (orange ball) is only affected in FGFR2-D2. For both receptors, an identical binding site of SSR was observed. For clarity, only one molecule of FGF and FGFR is shown. (B) For comparison, the binding sites of the saccharide heparin molecules are depicted in black/gray. The complex with heparin consists of two FGFs and FGFR-D2D3 molecules.

(C) Cartoon representation of the main binding mode of SSR to FGFR2-D2 (from NMR in this study, yellow; from MD modeling, pink) as predicted from free energy calculations and docking (left), with its corresponding binding free energy profile for SSR, as calculated by metadynamics (right). The low free binding energy corresponds to the low affinity (mM) of binding, as revealed by NMR studies. Binding of heparin is also shown.

(D) Overlay of the [^{1}H,^{15}N]-TROSY HSQC spectra, revealing CSPs induced by SSR on ^{15}N FGFR2-D2D3/FGF1 (top) and FGFR1-D1D2D3/^{15}N FGF2 (bottom); SSR-induced CSPs are indicated by arrows: black without SSR and red with SSR.

(E) CSPs induced by SSR in the experiments shown in (D) were mapped to the X-ray structure (1FQ9). Red balls denote residues showing CSP. Only one molecule of FGF and FGFR is shown.

(F) NMR titration experiments of the FGF1/FGFR1-D1D2D3 complex with SSR. Top: ^{1}H 1D signal of the SSR methoxy resonance. Black lines show the measured spectra; red lines indicate a least square fit using full signal simulation (performed by variation of K_D and k_{off}). Bottom: Chemical shift of the peak maximum (*x* axis) as a function of the ratio of complex to SSR concentration. Asterisks show the experimental values; the solid line results from a least square fit of the chemical shift data by variation of the reaction parameters.

See also Figure S2 and Table S2.

all domains was fully recovered by molecular replacement after separate deletion of single domains in the PDB file. In the presence of SR, the density of FGFR2-D3 was weak around a β sheet region (β2 at Asp^{272}-Val^{277} and β5 at Glu^{325}-Ile^{329}) located ~25 Å away from the orthosteric FGF-ligand-binding region in D3. Comparison of FGFR2-D2D3/FGF1 structures in the absence and presence of SR revealed no conformational differences. However, strong differences in the Debye-Waller factors (B-factors; higher values suggest flexibility) were observed. Surprisingly, the average B-factor of the X-ray protein structure in the presence of SR was strongly increased. Specific regions in FGFR2-D3 at β1β2 (Ala^{266}-Val^{277}) and α1β5 (Thr^{319}-Ile^{324}Glu^{325}-Ile^{329}) showed large decreases in the occupancy of atoms, resulting in high B-factors (Figure 4A). Together,

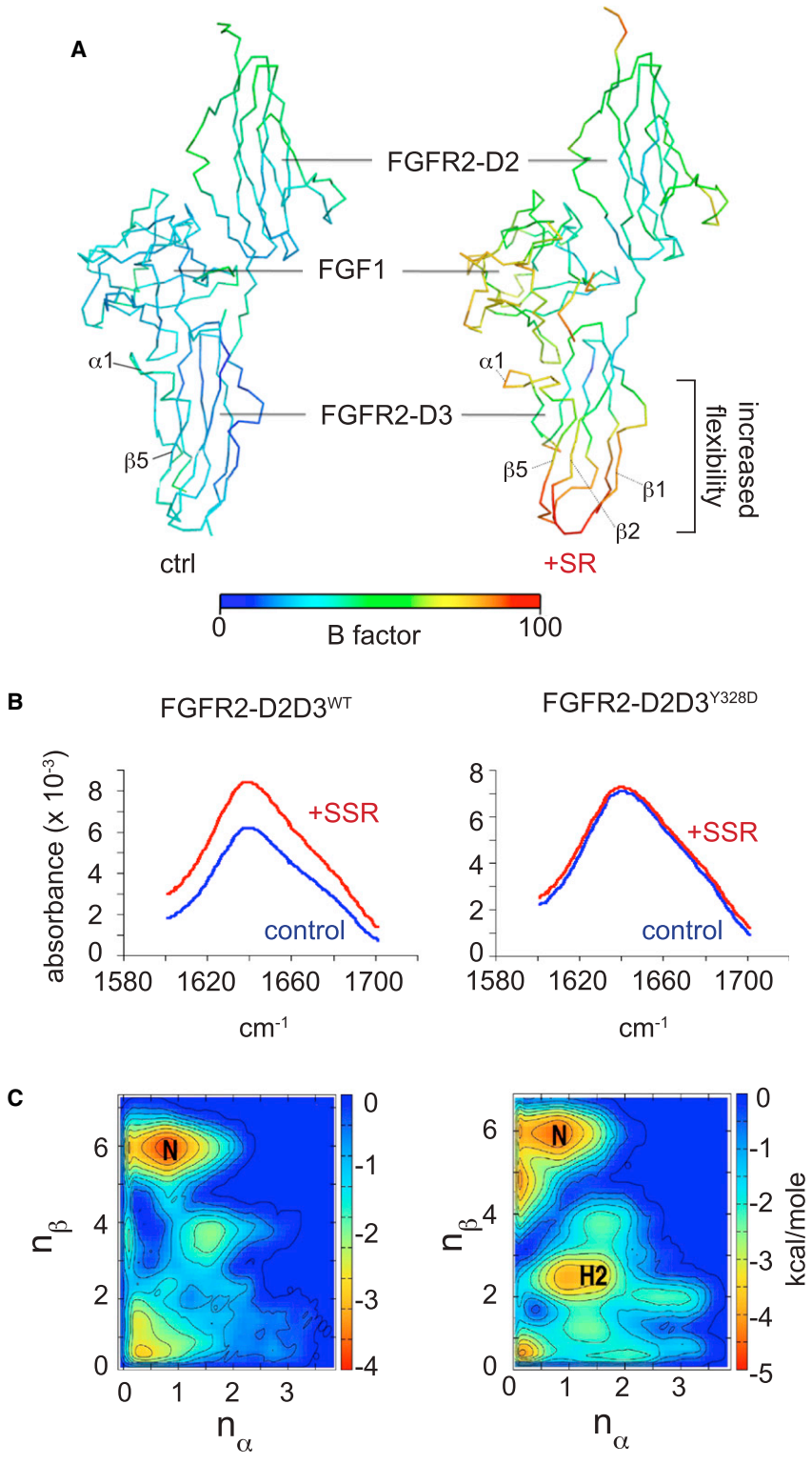

Figure 4. Crystallography, FTIR Analysis, and Free Energy Calculations

(A) 3D representation of the X-ray crystal structure of FGFR2-D2D3/FGF1 complex in the absence (left) and presence (right) of SR. The change in colors (B-factor values) suggests increased flexibility of D3 at α1/β5 after SR binding.

(B) FTIR measurements of FGFR2-D23^{WT} and FGFR2-D23^{Y328D} in the absence (blue) or presence (red) of SSR.

(C) Calculated free energy surfaces as a function of the β sheet and α helix content (nβ and nα, respectively; see Supplemental Information) in the absence (left) or presence (right) of SSR. The native state is marked with "N". Note the appearance of a new free energy minimum corresponding to the H2 state.

See also Figure S3.

the conformation of the FGF-FGFR complex and flexibility of FGFR2-D2 or FGF1 were not strongly affected by SR. However, TFZ scores, disturbed electron density maps, and increased B-factors suggest increased structural dynamics of D3, resulting from different conformational states induced by SR.

Mode of Action of SSR: Effect of SSR on FGFR-D3

The finding of an intrinsically disordered D3 domain in NMR studies and MD simulations together with the SR-induced increase of its B-factors in the X-ray structure led us to further investigate the influence of SSR on D3 using Fourier transform infrared (FTIR) spectroscopy and in silico methods. By obtaining an infrared spectrum of absorption, FTIR provides information on the transition from one to another conformation. Addition of SSR to FGFR2-D2D3 increased the amplitude of the amide I band in the FTIR spectrum with a maximum at 1,640 cm^{-1} (Figure 4B), suggesting that binding of SSR leads to a conformational change of FGFR-D2D3 (similar results were obtained when analyzing FGFR2-D1D2D3), in agreement with the AGADIR prediction.

We used state-of-the-art free energy (ΔG) calculations and computer modeling to unravel how the conformational landscape and flexibility of D3 changed in the presence of SSR. The free energy calculations were performed with the Gromacs 4 package and PLUMED plug-in using metadynamics, bias exchange metadynamics, and steered MD approaches and the Amber99SB*-ILDN force-field (Best and Hummer, 2009; Piana and Laio, 2007). Similar techniques were used previously to predict the free energy landscapes associated with conformational changes and ligand binding in kinases (Lovera et al., 2012; Saladino et al., 2012). Comparison of the free energy landscapes of D3 as a function of the β sheet and α helix content predicted that SSR stabilizes helix α1 (Thr^{319}-Ile^{324}) and induces a β sheet to α helix transition of part of β5 (Gln^{325}-Ile^{329}), thereby nearly doubling the number of turns in helix α1. As a result, D3 undergoes a conformational rearrangement into an intermediate

"H1" state, which progresses to state "H2," where a new hydrophobic cavity, not accessible in the native form of D3, is formed, in which the hydrophobic Tyr^{328} residue (solvent exposed in the native configuration) now faces the core of D3 (Figures 4C and S3C). The difference in free energy between the crystallographic fold of D3 and the refolded H2 state, calculated by two independent approaches (bias exchange metadynamics and steered MD simulations) was 2 to 3 kcal/mol. These data, in agreement with NMR and X-ray observations, suggest that D3 binds SSR and undergoes conformational rearrangements without becoming fully structured in the SSR-bound state.

Mode of Action of SSR: Helix-Breaker Mutations

To assess the importance of Tyr^{328} in the conformational changes of FGFR-D3, we mutated this residue to aspartate, which has known "helix-breaker" properties (to yield FGFR2-D2D3^{Y328D}, termed FGFR2^{Y328D}), as this mutation should reduce the helical tendency and impair the conformational change. Indeed, we hypothesized that the hydrophilic Asp^{328} would destabilize the α-helical conformation and that SSR would not be able to induce a conformational change in FGFR2^{Y328D}. FTIR revealed that FGFR2^{Y328D} did not exhibit a major shift in its spectrum in the absence of SSR, showing that its overall 3D configuration was preserved. Conformational analysis by FTIR showed, however, that SSR failed to induce a change in the spectrum of FGFR2^{Y328D} (Figure 4B). This effect was specific, as additional mutations of the Y328 residue (Y328R/I329K) still showed the same structural change as FGFR2^{WT} upon addition of SSR, illustrating that not any type of mutation of Y328 per se could rescue the SSR effects (data not shown).

The aforementioned observations suggest that SSR does not directly compete with FGF binding, but rather that it alters the conformational ensemble of FGFR-ECD, which allosterically propagates into receptor function changes. The β to α transition of the β5 helix (Glu^{325}-Ile^{329}) is critically involved in this allosteric effect. To assess the relevance of Tyr^{328} in transmitting SSR's allosteric activity, we generated HEK293 cell lines expressing wild-type FGFR2^{WT} or mutant FGFR2^{Y328D}. In the absence of SSR, FGFR2^{WT} and FGFR2^{Y328D} cells exhibited a similar ERK1/2 response to FGF2, showing that the mutation did not change FGFR's response to FGF. The mutation did also not alter orthosteric binding of ^{125}I-FGF2 (K_D: 54 ± 8 pM for FGFR2^{WT} versus 52 ± 9 pM for FGFR2^{Y328D}; n = 5; p = NS). However, SSR's ability to inhibit FGF2-induced ERK1/2 phosphorylation was reduced in FGFR2^{Y328D} cells (IC_{50} value: 121 ± 30 nM) as compared to FGFR2^{WT} cells (IC_{50} value: 28 ± 12 nM; $p < 0.05$) (Figures 5A and 5B). Similar data were obtained for FGFR2 phosphorylation and phospho-FRS2 signaling (Figures 5C and 5D).

We also stably overexpressed FGFR2^{WT} or FGFR2^{Y328D} in L6 myoblast cells (which lack endogenous FGFRs). Transduced cells were treated with AlexaFluor488-conjugated FGF2, leading to the formation of FGF2/FGFR2 at the cell membrane and its internalization in endocytic vesicles. Upon stimulation, FGFR2^{WT} and FGFR2^{Y328D} were comparably endocytosed (Figures 5E and 5F). Notably, SSR reduced endocytosis in FGFR2^{WT} but not in FGFR2^{Y328D} cells (Figures 5E and 5F). To unravel the endocytic pathway, inhibitors of clathrin- (Pitstop2) and caveolin-dependent (Dyngo-4a) pathways were used. Only Dyngo-4a affected endocytosis of FGFR2^{WT} and FGFR2^{Y328D}, indicating that the FGF2 endocytic pathway relies on caveolae-dependent internalization (Figures 5E and 5F), consistent with previous reports (Irschick et al., 2013). Thus, FGFR2^{WT} and FGFR2^{Y328D} showed similar profiles with respect to FGF2 affinity, ERK1/2 phosphorylation, and receptor internalization, but SSR inhibited signaling more efficiently in FGFR2^{WT} than FGFR2^{Y328D} cells. Thus, by altering the β to α transition of the β5 strand and thereby elongating the α1 helix, SSR modulates inhibition of FGFR signaling and internalization.

Mode of Action of SSR: Binding of SSR to D3 H2

Because of the flexibility in D3, we performed in silico binding studies using metadynamics, a recently developed method to dock ligands on receptors in water solution, allowing protein flexibility (Laio and Gervasio, 2008). This revealed that the free energy of binding to the hydrophobic cavity in the H2 state was −10.2 kcal/mol (Figure 6A), reflecting tight binding in the nM range. Overall, very long all-atom MD simulations and free energy calculations with metadynamics confirmed that SSR alters the flexibility and conformational propensity of D3. The stability of the helical region in FGFR2-D3 is enhanced by an initial step of low-affinity SSR binding, thereby making a new metastable H2 state accessible, which is stabilized by docking of SSR (Figures 6B–6D and S3C). Superposing D3′s structure in its SSR-bound H2 state with previously identified crystal structure of FGFR2-D2D3 showed that the FGF-interacting residues remain unaffected, in line with findings that SSR did not alter the affinity of FGFs.

In addition, free energy calculations showed that FGFR2^{Y328D} underwent helix elongation and adopted the conformational state H2, though H2 was less stable. This relates to the fact that stabilization of the cavity is largely due to interactions of the hydrophobic Tyr^{328} with the core of D3 and that these interactions are highly unfavorable in FGFR2-D3^{Y328D}, in which the hydrophilic Asp^{328} prefers solvent exposure rather than buried conformations. Our finding that Y328D reduces but does not eliminate SSR binding explains why FGFR2^{Y328D} is still capable of binding SSR but also why its signaling is inhibited less by SSR.

Structure-Activity Relationship Analysis

Experimental and computational approaches suggest a nonconventional allosteric regulation of FGFR function by binding of SSR to the disordered ensemble of D3. MD simulations outline the major structural features of the H2 state and schematic features of the arising binding cavity. To further probe the molecular details of the D3-SSR interaction, we analyzed the structure activity relationship (SAR) of a set of 19 SSR analogs by comparing their biological activity (inhibition of phospho-ERK1/2 signaling) to their capacity to dock into the in silico-identified binding pocket of D3 (H2 state) using the Schrödinger Glide XP package on the nonflexible H2 state of FGFR2-D3. As shown in Table S3, two active SSR analogs inhibited ERK1/2 phosphorylation with a comparable efficiency as SSR ($IC_{50} \sim$ 10–100 nM); their activity was reduced in FGFR2^{Y328D} cells (Table S4), confirming the specificity of their activity. Six other compounds had weak biological activity ($IC_{50} \sim$ 100–1,000 nM), while another ten molecules were inactive ($IC_{50} >$ 1,000 nM). One compound could not be tested because of insolubility. Docking experiments showed that the binding energy generally correlated

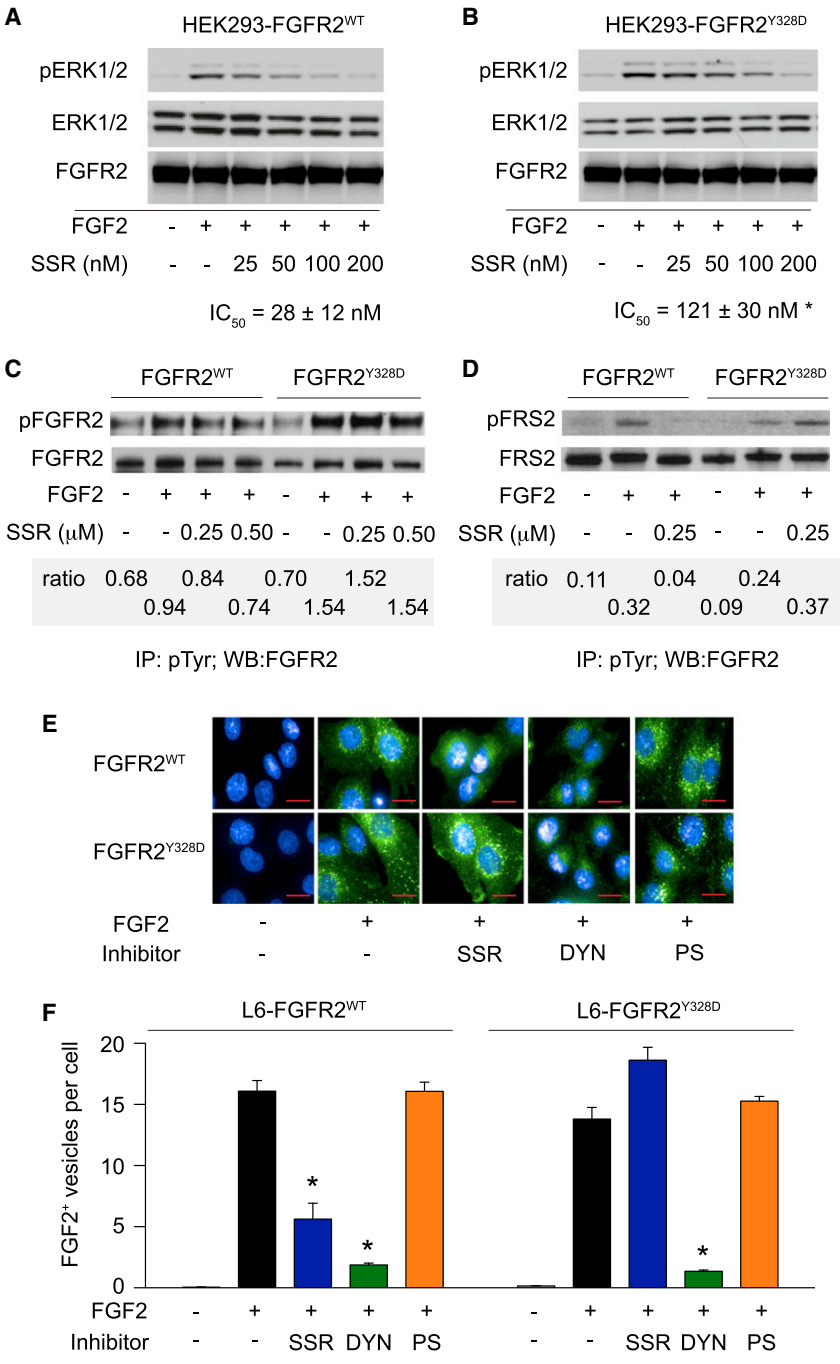

Figure 5. FGFR Signaling in FGFR2^{WT} and FGFR2^{Y328D} Cells

(A–D) Analysis of inhibition of FGFR2^{WT} or FGFR2^{Y328D} by SSR in HEK293 cells stably expressing these proteins using immunoblot. Phosphorylated ERK1/2 (pERK1/2) and total ERK1/2 (ERK1/2), upon FGF2 stimulation, were determined and ratios of pERK1/2 over total ERK1/2 were used to calculate IC_{50} values (A and B; mean ± SEM, n = 3). The asterisk indicates $p < 0.05$ versus FGFR2^{WT}. FGFR2 was used as loading control. Similar results were obtained when analyzing phosphorylation of FGFR2 (C) and FRS2 (D) upon prior immunoprecipitation for phosphotyrosine (pTyr) residues (the ratio of phospho- over total protein is shown).

(E and F) Analysis of endocytic vesicle formation in L6 myoblasts stably expressing FGFR2^{WT} or FGFR2^{Y328D} and stimulated with AlexaFluor488-conjugated FGF2 in the presence of control, SSR (1 μM), Dyngo-4a (3 μM, DYN), or Pitstop2 (1 μM, PS). Representative images are shown in (E) (scale bars: 20 μm), and the result of quantification of the number of AlexaFluor488-conjugated FGF2 endocytic vesicles is shown in (F). Each bar corresponds to the number of vesicles detected on 28–30 views from three different wells (mean ± SEM; n = 3). The asterisk indicates $p < 0.05$ versus FGF2 alone.

with biological inhibition and that the binding strength of the active compounds was significantly higher than of the weak and inactive compounds (Figure S4A).

Computational modeling suggested that several critical substitutes were adjacent to residues in the Thr^{319}-Arg^{330} region (i.e., R1 and R2 in the vicinity of Leu^{327}-Tyr^{328}-Ile^{329} and R′ and R″ pointing toward Thr^{319}-Thr^{320}-Glu^{323}-Ile^{324}; Figure 7A). More detailed analysis revealed the following insights (Table S3): (1) R′ group: a carboxylate group (or amide bioisostere) at R′ is required for full biological activity (compound 7); changing this group abrogated SSR's activity (compounds 10–13,16); switching the carboxyl group at R′ and the aniline group at R″ retains residual activity (compound 5), likely because of sufficient docking, but this configuration is less favorable because one charge-charge interaction (with Lys^{279}) and a H-bond between neutral groups (Thr^{319}, Thr^{320}) are replaced with H-bond interactions between charged and neutral groups; (2) R″ group: the aniline group is required as its removal (compound 4 and 17) or monomethylation (compound 6) lowered the activity, in line with the observation that these compounds had reduced polar and H-bond interactions in the H2 state; (3) R1 group: switching the methoxy group for a carboxyl group prevents docking into the H2 pocket (compound 11), but this group can be replaced by a hydrogen atom without losing activity (compound 3), highlighting the need for hydrophobic interactions not compatible with negative charge; and (4) R2 group: the methyl group can be substituted by a cyclopropyl group, retaining potency consistent with comparable hydrophobic interactions with the pocket (compound 2).

These data confirm that the Thr^{319}-Arg^{330} region is important for SSR binding and transduction of the allosteric information. Noteworthy, the R1 moiety facing Tyr^{328} is critical, explaining why SSR binding and inhibitory activity were impaired by the bulky methoxybenzamide and methoxybenzenesulfonamide at R1 (compounds 17 and 18). Likewise, the bulky CONHMe at R6 (compound 8) is not tolerated, probably because of steric clashes with the hydrophobic pocket. Other substitutions

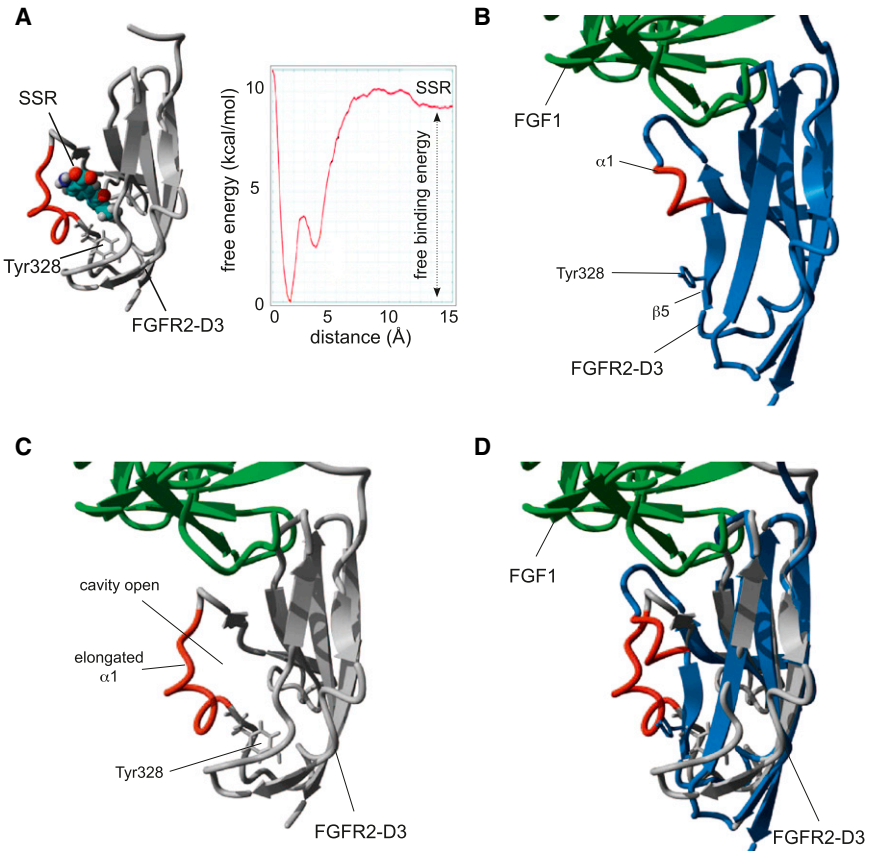

Figure 6. Free Energy Calculations and Conformational States

(A) Cartoon representation of the main binding mode of SSR to FGFR2-D3, as predicted from free energy calculations and docking (left) and the corresponding binding free energy profile for SSR as calculated by metadynamics (right).

(B–D) Cartoon representation of the conformation adopted by FGFR2-D3 in the native state (without SSR) (B) and in the H2 state in the presence of SSR (C), as obtained by calculating the free energy using molecular dynamics modeling (for reasons of clarity, SSR itself is not shown); the overlay is shown in (D). Note the elongated helix α1 and the position of Tyr^{328} pointing toward the hydrophobic core of the domain in the H2 state compared to the native state. FGF1, green; native FGFR2-D3, blue; FGFR2-D3 "H2" conformation, gray; helix α1, red.

abrogated the function, even though they did not interfere much with binding itself, which is compatible with the allosteric mode of action, in a sense that not binding per se but rather the conformational change induced by the SSR derivative matters.

On a subset of active, weak, and inactive compounds (Table 1), we performed biophysical (STD-NMR and waterLOGSY-NMR; Bretonnet et al., 2007) experiments to assess their binding capacity to FGF1/FGFR2-D2D3. Also, to allow flexibility of protein movements, we calculated the free binding energy (ΔG) of these compounds using metadynamics, which, in contrast to standard modeling on a rigid structure, also takes into account movements of the protein. The agreement between the calculated ΔG and biological activity is superior to that obtained with the Glide XP score (Table 1; Figures 7B and S4B). For instance, when we subtract the thermodynamic penalty of state H2 (2 to 3 kcal/mol) from the calculated binding free energies, we obtained −8/−9 and −9/−10 kcal/mol for SSR and compound 2, which is in very close agreement with the expected value of −8.5 kcal/mol for compounds in the 100 nM affinity range. An agreement is also obtained for weak and inactive compounds. The superior agreement of the free energy (calculated by Metadynamics) over the docking scores (calculated by Glide XP) stresses the importance of considering flexibility and explicit water hydration.

This view is also supported by NMR measurements, in which STD and waterLOGSY NMR were used to rank binding of this subset of compounds (Table 1). The NMR data are in good agreement with the calculated binding energy values and biological potency. Two compounds from the active group bound the strongest, and SSR itself was the third strongest binder, which also underscores that, besides binding strength itself, the compatibility with the structural allosteric transition is also important for the effect of the compound. Again, adding large groups at R1 induces the most profound effect (compound 17 being the weakest and compound 18 being undetectable by NMR due to protein precipitation). Overall, the binding affinity of SSR variants and their allosteric effect of binding generally correlate: the stronger a derivative binds, the more it drives the conformation of the receptor toward the inhibited ensemble.

DISCUSSION

In the accompanying paper (Bono et al., 2013), we identified SSR, a synthetic inhibitor of the FGF tyrosine kinase receptor, and provided pharmacological evidence for an allosteric mechanism. This orally deliverable, small-molecule, multi-FGFR inhibitor showed promising therapeutic anticancer efficacy (Bono et al., 2013). SSR does not affect orthosteric FGF ligand binding, cannot penetrate the membrane, and does not directly block the TK activity but exhibits typical pharmacological allosteric features. Indeed, the compound shows signaling bias by inhibiting ERK1/2 activation (relying on FGFR internalization) without altering phospholipase C (PLC)-γ phosphorylation, has a "ceiling" effect, and exhibits "probe dependence" (Bono et al., 2013). All these findings suggest an allosteric conformational effect that discriminatively affects the readout of receptor activation. In this study, efforts were made to unravel the molecular mechanisms of the allosteric activity of SSR. The challenge in these investigations is due to both the complexity of the FGFRs and the disordered, even unfolded nature of domain D3, which is prone to aggregation, invisible to NMR, and highly flexible in the X-ray structures in the presence of SSR.

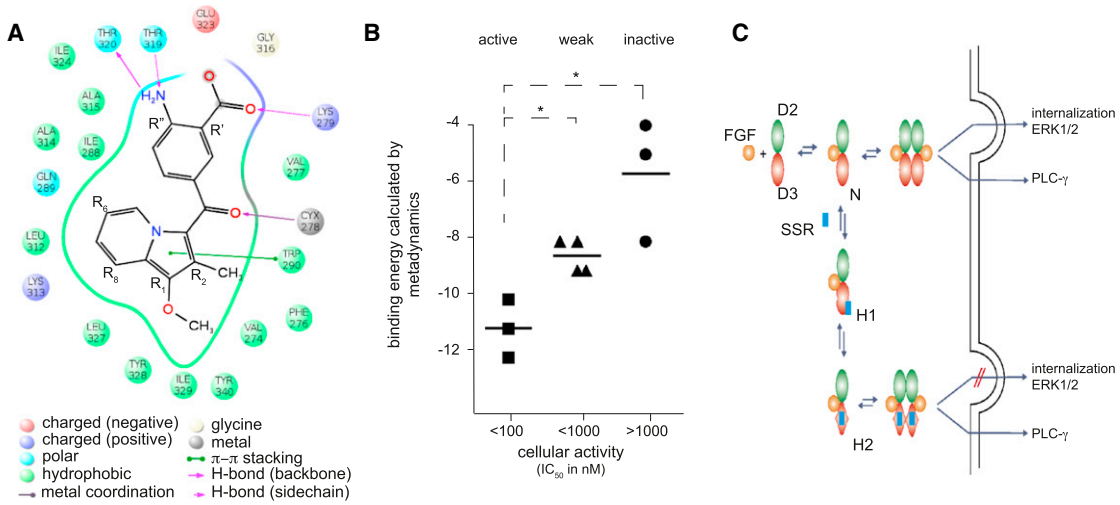

Figure 7. SAR and Hypothetical Model of the Allosteric Regulation of FGFR by SSR

(A) Scheme of the putative SSR binding pocket in the newly exposed cavity in the H2 state, used for the docking analysis to obtain the SAR. The position and type of individual amino acid residues and putative interactions are indicated. The colored band lining the cavity represents hydrophobicity (green is hydrophobic; blue is charged).

(B) Scatterplot analysis of calculated binding energy using metadynamics of the three different classes of compounds from the SAR analysis. The compounds of each group are shown in Table 1. The asterisk indicates $p < 0.05$ between the indicated conditions (dashed lines); horizontal full lines represent averages.

(C) Under normal conditions, heparin sulfate-bound FGF (orange circle) binds to FGFR ECD via D2 (green) and D3 (red). While D2 is well folded, D3 is in a disordered native (N, probably corresponding to a molten globule) state. The receptor can dimerize and induce distinct intracellular signaling pathways, such as receptor internalization (leading to ERK1/2 phosphorylation) and PLC-γ phosphorylation. Due to its inherent flexibility, D3 can transit to an alternative disordered state (H1), which is more open and competent for weak SSR binding. From this state, there is a transition to a third disordered state (H2), which binds SSR stronger. In this state, SSR does not inhibit FGF binding or dimerization, but, due to altering the conformational ensemble and/or dynamics of D3, it inhibits receptor internalization. Allostery of the system arises from SSR acting indirectly via long-range conformational effects in the disordered ensemble, attenuating membrane interaction.

See also Figure S4 and Tables S3 and S4.

At first, it may appear surprising that a small molecule like SSR is capable of inhibiting the responses of various FGFRs to multiple FGF ligands if steric hindrance of the orthosteric FGFR pocket was the desired mode of receptor targeting. However, an allosteric interaction with a small molecule can perturb the signaling of a large FGF ligand by inducing a conformational change in FGFR. The model that emerges from computer simulations and modeling reconciles the experimental findings by predicting a marginally stable D3 fold, a weak SSR binding site on D2, and a conformational change in D3 in the presence of SSR. The AGADIR software also independently predicted a conformational preference of α helix over β sheet structure. The conformational change gives rise to a new hydrophobic cavity, to which SSR can bind. A mutation that reduced the α-helical propensity in this region was predicted to suppress the SSR-induced conformational changes in silico and indeed counteracted SSR's ability to inhibit FGFR-driven cellular processes.

The key element of the model is the allosteric nature of SSR's action. Whereas this molecule was selected by using the SPA assay for FGF binding and has nM pharmacological effects, it does not interfere with FGF binding or receptor dimerization in a cellular context. Because SSR is not internalized, it acts on the extracellular part of the receptor. Direct SSR binding to FGFR was indeed demonstrated experimentally, as was the conformational change that is critical for affecting receptor function. Allostery also follows from the "ceiling" effect, the differential effect on distinct downstream signaling pathways, and "probe dependence" (Bono et al., 2013). All these observations can be reconciled with data from structural experiments and modeling calculations in the following model: (1) an SSR-induced conformational rearrangement of D3 is suggested by most techniques; (2) structural disorder of D3 is confirmed by NMR, MD simulations, and high-crystallographic B-factors; and (3) defective receptor internalization in the presence of SSR is shown in cellular assays and suggested by differential pharmacological effects.

Therefore, the structural underpinning of the system is that the actual structural state of domain D3 is probably a conformational ensemble corresponding to a MG state, with a global topology resembling the structure stabilized in crystallography. This domain thus falls into the growing family of intrinsically disordered proteins, which lack well-defined stable folds, yet play key regulatory and signaling roles in many cellular processes (Tompa, 2011). Its dimerization, even without a folding transition, can be envisaged, as in fuzzy complexes (Tompa and Fuxreiter, 2008) such as T-cell receptor zeta (Duchardt et al., 2007; Sigalov et al., 2004). As is the case with MG states, its various conformations are in an intermediate kinetic exchange regime that causes severe line broadening in NMR, making it invisible to the NMR (Park et al., 2011).

The native ensemble of D3 samples the minor state H1, in which the β5 region tends to adopt local helical conformations; this structural state is stabilized by weak interactions

Table 1. Structure Activity Relationship of SSR Analogs

Compound	R_1[a]	R_2	R′	R″	pERK Inhibition (IC_{50} Range, nM)[b]	ΔG of Binding (calculated, kcal/mol)	Glide XP Score	NMR Binding Event (fSTD/fWL)
Active								
1 (SSR)	OMe	Me	COOH	NH_2	<100	−11	−10.3	2.0/3.8
2	OMe	cPr	COOH	NH_2	<100	−12	−11.3	4.9/15.0
3	H	Me	COOH	NH_2	<100	−10[c]	−11.3	4.4/12.6
Weak								
5	OMe	Me	NH_2	COOH	<1,000	−8	−8.2	1.5/3.2
6	OMe	Me	COOH	NHMe	<1,000	−9	−9.8	3.8/11.6
7	OMe	Me	$CONH_2$	NH_2	<1,000	−9	−9.1	ND
9	Et	Me	COOH	NH_2	<1,000	−8	−12	ND
Inactive								
13	OMe	Me	COOMe	NH_2	>1,000	−8	−10.3	ND
14	OMe	Me	COOH	OH	>1,000	−5	−11.9	ND
17	3-Methoxybenzamide	Me	COOH	H	>1,000	−4	−4.7	0.7/1.9
18	3-Methoxybenzene-sulfonamide	Me	COOH	NH_2	>1,000	ND	−4.2	Not detectable

Compound 1 is SSR. ND, not determined; fSTD, STD amplification factor; fWL, quantitative waterLOGSY effect.
See also Tables S3 and S4.
[a]The position of the groups (R′, R″, R^1, R^2) is indicated in the chemical structure in Figure 7A.
[b]The inhibition of ERK1/2 phosphorylation was determined for four concentrations of each compound (i.e., 1, 10, 100, and 1,000 nM).
[c]A major induced fit effect on D3 is observed, increasing the uncertainty on this estimate.

with SSR, as indicated by an increase of B-factors upon SR binding, MD simulations, and FTIR. Local helical conformations are also underlined by AGADIR predictions. Overall, this transition is compatible with the ability of small molecules to bind to the disordered state, as observed in the inhibition of Myc-Max heterodimerization (Metallo, 2010). The SSR-FGFR interaction is likely heterogeneous, as suggested by the failure of observing electron density for the bound SR in the crystal structure.

MD simulations suggest that, upon transition to this transient and heterogeneous complex, a hydrophobic cavity becomes exposed, in which Tyr^{328} plays a key role. This transient complex may then relax into a more stable structural ensemble (H2), in which SSR is buried in the hydrophobic cavity (Figure S3C). This results in a much stronger interaction, which does not inhibit FGF binding but alters FGFR signaling, possibly due to interfering with membrane binding and/or internalization (Figure 7C). Disorder of this state is confirmed by increased crystallographic B-factors in the SR-complex and MD simulations and is also compatible with the allosteric nature of regulation of the receptor. Transitions in the ensemble N → H1 → H2 translate into different interactions with the membrane and/or different dynamics and orientations of receptor subunits in the dimer, resulting in inhibition of receptor internalization but not PLC-γ phosphorylation. In all, this scenario is fully compatible with recent concepts of allostery, which emphasize the importance of changes in dynamics without alteration of the equilibrium conformation (Tzeng and Kalodimos, 2009), and/or redistribution of the ensemble of intrinsically disordered protein structures (Hilser and Thompson, 2007). The outcome of these transitions, as seen in in cellulo assays, is an inhibition of slow and irreversible FGF-dependent receptor endocytosis abolishing ERK1/2 phosphorylation. A similar allosteric mechanism was described for the ganglioside GM3 and EGF receptor; the latter is closely related to FGFR (Coskun et al., 2011).

The allosteric effect was also confirmed by SAR analysis, which shows a good correlation of binding free energies of various SSR derivatives and their allosteric inhibition calculated by metadynamics modeling, while the docking scores, with their known limitations, also have an overall correlation with biological activity. This behavior would be fully incompatible with an orthosteric competitive inhibition of FGF binding and can be best explained by a binding model in which the allosteric activity of the compound stems from its ability to induce the proper shift in the conformational ensemble of the receptor. In most cases, altering substituent R1, which faces Tyr^{328}, impairs the allosteric activity of the compound, which points to the importance of this residue in the allosteric transitions.

Mutagenesis studies of Tyr^{328} are also in line with this conclusion, because the Tyr to Asp replacement does not basically affect the D3 structural ensemble, leaving its FGF-binding capacity and dimerization intact. On the other hand, it reduces the capacity of the structure to sample the local helical conformations, characteristic of H1 (and H2) states, thus altering SSR binding and its ability to interfere with signaling. This is in line with our FTIR experiments, MD simulations, and cellular assays. In addition, this disorder-based binding and allosteric mechanism is also compatible with the relaxed specificity of SSR, which is capable of interfering with different FGFR variants in distinct species. This would be difficult to reconcile with a well-folded (preformed) binding cavity on D3, which would limit FGFR isoform specificity toward SSR. Adaptability of the structural ensemble of intrinsically disordered proteins in binding is observed in many cases (Dunker et al., 2008). A corollary of this conserved allosteric regulation in all FGFR structures is that the receptor may have endogenous regulatory compound(s)

that act by a similar mechanism; identifying these molecules may open exciting avenues of FGFR research.

A final word is due on the difference of Ki values observed in the distinct in vitro and in vivo experiments. Such an enhanced response to small-molecule effectors in vivo is often observed (Hanoulle et al., 2007; Huppa et al., 2010), probably due to cellular conditions, such as the presence of additional (protein) factors or the vicinity of the membrane. The latter is probably signaled by the preferential inhibitory effect on receptor internalization rather than PLC-γ phosphorylation. In the case of FGFR, this effect may be augmented by the structural sensitivity of the conformational ensemble of the D3 domain.

What are the possible implications of this study? From a structural biology perspective, our study provides insight in fundamental mechanisms of how FGFRs transmit signals and provides unprecedented evidence for allosteric regulation of growth factor receptor tyrosine kinases. We show the importance of taking into account target flexibility in order to understand the mode of action of allosteric ligands. In addition, from a biopharmaceutical perspective, our results unveil the therapeutic potential for FGFR antagonists, perhaps wider than previously attributed to tyrosine kinase inhibitors, since SSR blocks not one but multiple FGFRs and because allosteric modulators are considered to have an improved benefit/risk ratio and to offer opportunities for fine-tuning biological responses in a manner that is not attainable with classic orthosteric modulators (Christopoulos, 2002). Finally, our results show that development of orally deliverable selective allosteric inhibitors of growth factor receptors is feasible, which creates formidable therapeutic opportunities for the future.

EXPERIMENTAL PROCEDURES

Compound Reconstitution

SSR was stored as pure powder at 4°C in the dark. For the different assays, SSR was dissolved in DMSO at a concentration of 100 mM and stored at −20°C until further use. SU5402 (Calbiochem) was also dissolved in DMSO at a concentration of 10 mM and stored at −20°C. For each assay, the same amount of DMSO was used for the control condition.

Materials

FGF1 and FGF7 were purchased from R&D Systems and FGF2 was produced and purified in-house. Human umbilical vein endothelial cells (HUVECs) are single-donor HUVECs from Promocell.

Cell Survival

Apoptotic cells were detected using fluorescein isothiocyanate-conjugated annexin V. Each assay was performed in triplicate and repeated three times.

FGFR2 Kinase Assay

Kinase activity measurements of the recombinant catalytic domain of FGFR2 was done using the ADP-Glo Kinase Assay and the Cyclex FGFR2 Kinase Assay/ Inhibitor screening kit (Sanbio, Uden, The Netherlands) according to the manufacturer's protocol.

Confocal Microscopy Studies

EEA-1 labeling was performed on HUVECs or SNU-16 cells starved for 24 hr in 1% fetal bovine serum containing medium and stimulated for 2 hr with FGFs diluted in prewarmed medium without fetal calf serum in the presence or absence of SSR. Cells were then rinsed with cold PBS and fixed for 15 min with paraformaldehyde 4% and then permeabilized with PBS-Triton 0.1% for 5 min. Following washing with cold PBS, nonspecific sites were saturated with 1% normal goat serum (Zymed) in PBS for 1 hr at room temperature. Early endosomal vesicles were detected using mouse anti-human EEA1 antibody (1/100, BD Biosciences) overnight at 4°C and revealed with AlexaFluor488-conjugated anti-mouse antibody (1/2,000, Invitrogen) for 2 hr at 4°C. Wells were rinsed twice with 1 ml PBS. Then, all liquids were removed and one drop of Fluoprep (Biomerieux) was added and mounted with a round coverslip (KnittelGläser). Confocal microscopy views were performed with a Zeiss LSM510. The number of EEA1-positive vesicles around the nucleus was counted with Columbus software (PekinElmer). For FGF-R4 staining, HUVEC were only fixed with Dako Cytomaton kit following supplier recommendations. FGF-R4 was detected with primary anti-FGFR4 MAB685 (1/100, R&D Systems).

Western Blot Analysis and Phosphoproteome Profiler Array

These studies were realized on 24 hr-starved cells that were then stimulated for 7 min with FGFs in the presence or absence of SSR. Immunoblots were carried out with anti-phosphoprotein antibodies against FGFRs (Santacruz Biotech, Sc30262), FRS2 (Cell Signaling Tech., 3864), Erk1/2 (Cell Signaling Tech., 4377), or anti-glyceraldehyde 3-phosphate dehydrogenase (GAPDH) (Cell Signaling Tech., 2118). The proteome array was run in accordance with supplier recommendations.

FTIR Measurements

FTIR was performed using a Bruker Tensor 37 FTIR spectrometer equipped with an AquaSpec flow cell. The sample compartment was thermostatted to 25°C and 100 spectra were averaged for a good signal-to-noise ratio. Proteins were purified as described in Supplemental Experimental Procedures. Immediately after the gel filtration, the proteins were dialyzed overnight in the same preparation of buffer (10 mM 4-[2-hydroxyethyl]-1-piperazineethanesulfonic acid pH 7.2, 150 mM NaCl) in the presence or absence of SSR. Dialysis buffer samples were used to subtract background signal. The analysis was performed using the OPUS software package provided by Bruker.

STD- and 1D-NMR Measurements

All STD- and 1D-NMR experiments were carried out on a BRUKER three-channel DRX600 and on a BRUKER four-channel DRX800 spectrometer at the standard temperature of 298 K and were referenced to the internal standard 3-trimethyl-2,2,3,3-tetradeuteropropionate sodium salt. A detailed description has been included in the Supplemental Information.

X-Ray Crystallography

Crystals of FGF1/FGFR2 D2D3 complexes with and without SR/SSR compounds could be obtained under crystallization conditions containing 0.1 M Tris/HCl pH 8, 1.8 M $(NH_4)_2SO_4$ at protein concentration of 2 mg/ml. Crystals with SSR diffracted up to 6 Å, whereas SR bound crystals diffracted up to 4 Å at SLS Villingen. Data could be integrated using XDS and phased with Phaser, using MR of separate domains FGF1, FGFR2 D2, and FGFR2 D3 of the crystal structure 1E0O. Because of bad resolution, all residues were mutated to alanine. The poly-A backbone model of FGF1/FGFR2 D2D3 was refined using Refmac5 and Coot.

In Silico Molecular Modeling and Metadynamics Modeling

All the detailed procedures are in the Supplemental Information.

Other Assays

For methods such as cell proliferation, survival, FGFR kinase assay, confocal microscopy, FTIR, and western blotting, we used standard protocols that are detailed in the Supplemental Experimental Procedures.

Statistics

All data represent the mean ± SEM of the indicated number of experiments. Statistical significance was calculated by Student's t test, considering $p < 0.05$ as statistically significant.

ACCESSION NUMBERS

The low resolution polyA backbone model of the FGFR2D2D3/FGF1/SSR128545 complex has been deposited in the RCSB Protein Data Bank under the ID code rcsb077498 and PDB ID code 4J23.

SUPPLEMENTAL INFORMATION

Supplemental Information includes four figures, four tables, and Supplemental Experimental Procedures and can be found with this article online at http://dx.doi.org/10.1016/j.ccr.2013.02.018.

ACKNOWLEDGMENTS

The authors would like to thank J. Fidelak for his contribution and L. Notebaert for help with the figures. G.S. and F.L.G. acknowledge partial support by Spanish Science and Innovation grant BIO2010-20166. F.D.S. was supported by the Flemish Institute for the Promotion of Scientific Research (IWT) and the Flemish Foundation for Scientific Research (FWO) Belgium. This work was also supported, in part, by grant numbers G.0567.05 and G.0405.05 from the FWO, Belgium; grant number GOA/2006/11 from the Concerted Research Activities, Belgium; grant number LSHG-CT-2004-503573 from the EU 6th Framework Program; the Belgian Science Policy (IAP numbers P5-02 and P6-30); and by long-term structural Methusalem funding from the Flemish Government (to P.C.). Funding for H.S. was derived from EXC 115 DFG, Cluster of Excellence: Macromolecular Complexes.

C.H., C.A., M.B., D.S., P.R., J.P.H., G.L., J.M.H., F.B. are employees of Sanofi-Aventis, Montpellier, France. P.C., J.S., F.R., F.D. are inventors on the international patent application "extracellular allosteric inhibitor binding domain from a tyrosine kinase receptor" with publication number WO2011/001413 and its national counterparts.

Received: July 24, 2012
Revised: December 12, 2012
Accepted: February 19, 2013
Published: April 15, 2013

REFERENCES

Beenken, A., and Mohammadi, M. (2009). The FGF family: biology, pathophysiology and therapy. Nat. Rev. Drug Discov. *8*, 235–253.

Belleudi, F., Leone, L., Nobili, V., Raffa, S., Francescangeli, F., Maggio, M., Morrone, S., Marchese, C., and Torrisi, M.R. (2007). Keratinocyte growth factor receptor ligands target the receptor to different intracellular pathways. Traffic *8*, 1854–1872.

Best, R.B., and Hummer, G. (2009). Optimized molecular dynamics force fields applied to the helix-coil transition of polypeptides. J. Phys. Chem. B *113*, 9004–9015.

Bono, F., De Smet, F., Herbert, C., DeBock, K., Georgiadou, M., Fons, P., Tjwa, M., Alcouffe, C., Ny, A., Bianciotto, M., et al. (2013). Inhibition of tumor angiogenesis and growth by a small-molecule multi-FGF receptor blocker with allosteric properties. Cancer Cell *23*, this issue, 477–488.

Bretonnet, A.S., Jochum, A., Walker, O., Krimm, I., Goekjian, P., Marcillat, O., and Lancelin, J.M. (2007). NMR screening applied to the fragment-based generation of inhibitors of creatine kinase exploiting a new interaction proximate to the ATP binding site. J. Med. Chem. *50*, 1865–1875.

Christopoulos, A. (2002). Allosteric binding sites on cell-surface receptors: novel targets for drug discovery. Nat. Rev. Drug Discov. *1*, 198–210.

Conn, P.J., Christopoulos, A., and Lindsley, C.W. (2009). Allosteric modulators of GPCRs: a novel approach for the treatment of CNS disorders. Nat. Rev. Drug Discov. *8*, 41–54.

Coskun, U., Grzybek, M., Drechsel, D., and Simons, K. (2011). Regulation of human EGF receptor by lipids. Proc. Natl. Acad. Sci. USA *108*, 9044–9048.

Duchardt, E., Sigalov, A.B., Aivazian, D., Stern, L.J., and Schwalbe, H. (2007). Structure induction of the T-cell receptor zeta-chain upon lipid binding investigated by NMR spectroscopy. ChemBioChem *8*, 820–827.

Dunker, A.K., Oldfield, C.J., Meng, J., Romero, P., Yang, J.Y., Chen, J.W., Vacic, V., Obradovic, Z., and Uversky, V.N. (2008). The unfoldomics decade: an update on intrinsically disordered proteins. BMC Genomics *9*(*Suppl 2*), S1.

Gasparini, G., Longo, R., Toi, M., and Ferrara, N. (2005). Angiogenic inhibitors: a new therapeutic strategy in oncology. Nat. Clin. Pract. Oncol. *2*, 562–577.

Hanoulle, X., Melchior, A., Sibille, N., Parent, B., Denys, A., Wieruszeski, J.M., Horvath, D., Allain, F., Lippens, G., and Landrieu, I. (2007). Structural and functional characterization of the interaction between cyclophilin B and a heparin-derived oligosaccharide. J. Biol. Chem. *282*, 34148–34158.

Hilser, V.J., and Thompson, E.B. (2007). Intrinsic disorder as a mechanism to optimize allosteric coupling in proteins. Proc. Natl. Acad. Sci. USA *104*, 8311–8315.

Huppa, J.B., Axmann, M., Mörtelmaier, M.A., Lillemeier, B.F., Newell, E.W., Brameshuber, M., Klein, L.O., Schütz, G.J., and Davis, M.M. (2010). TCR-peptide-MHC interactions in situ show accelerated kinetics and increased affinity. Nature *463*, 963–967.

Irschick, R., Trost, T., Karp, G., Hausott, B., Auer, M., Claus, P., and Klimaschewski, L. (2013). Sorting of the FGF receptor 1 in a human glioma cell line. Histochem. Cell Biol. *139*, 135–148.

Laio, A., and Gervasio, F.L. (2008). Metadynamics: a method to simulate rare events and reconstruct the free energy in biophysics, chemistry and material science. Rep. Prog. Phys. *71*, 126601.

Lovera, S., Sutto, L., Boubeva, R., Scapozza, L., Dölker, N., and Gervasio, F.L. (2012). The different flexibility of c-Src and c-Abl kinases regulates the accessibility of a druggable inactive conformation. J. Am. Chem. Soc. *134*, 2496–2499.

McCoy, A.J., Grosse-Kunstleve, R.W., Adams, P.D., Winn, M.D., Storoni, L.C., and Read, R.J. (2007). Phaser crystallographic software. J. Appl. Cryst. *40*, 658–674.

Metallo, S.J. (2010). Intrinsically disordered proteins are potential drug targets. Curr. Opin. Chem. Biol. *14*, 481–488.

Murshudov, G.N., Dodson, E.J., and Vagin, A.A. (1996). Application of maximum likelihood methods for macromolecular refinement. In CCP4 Study Weekend Proceedings: Macromolecular RefinementCCP4 Study Weekend Proceedings: Macromolecular Refinement (Warrington, United Kingdom: Daresbury Laboratory), pp. 93–104.

Overington, J.P., Al-Lazikani, B., and Hopkins, A.L. (2006). How many drug targets are there? Nat. Rev. Drug Discov. *5*, 993–996.

Park, S.J., Borin, B.N., Martinez-Yamout, M.A., and Dyson, H.J. (2011). The client protein p53 adopts a molten globule-like state in the presence of Hsp90. Nat. Struct. Mol. Biol. *18*, 537–541.

Pellegrini, L., Burke, D.F., von Delft, F., Mulloy, B., and Blundell, T.L. (2000). Crystal structure of fibroblast growth factor receptor ectodomain bound to ligand and heparin. Nature *407*, 1029–1034.

Piana, S., and Laio, A. (2007). A bias-exchange approach to protein folding. J. Phys. Chem. B *111*, 4553–4559.

Plotnikov, A.N., Schlessinger, J., Hubbard, S.R., and Mohammadi, M. (1999). Structural basis for FGF receptor dimerization and activation. Cell *98*, 641–650.

Reilly, J.F., Mizukoshi, E., and Maher, P.A. (2004). Ligand dependent and independent internalization and nuclear translocation of fibroblast growth factor (FGF) receptor 1. DNA Cell Biol. *23*, 538–548.

Saladino, G., Gauthier, L., Bianciotto, M., and Gervasio, F.L. (2012). Assessing the performance of metadynamics and path variables in predicting the binding free energies of p38 inhibitors. J. Chem. Theory Comput. *8*, 1165–1170.

Schlessinger, J., Plotnikov, A.N., Ibrahimi, O.A., Eliseenkova, A.V., Yeh, B.K., Yayon, A., Linhardt, R.J., and Mohammadi, M. (2000). Crystal structure of a ternary FGF-FGFR-heparin complex reveals a dual role for heparin in FGFR binding and dimerization. Mol. Cell *6*, 743–750.

Sigalov, A., Aivazian, D., and Stern, L. (2004). Homooligomerization of the cytoplasmic domain of the T cell receptor zeta chain and of other proteins containing the immunoreceptor tyrosine-based activation motif. Biochemistry *43*, 2049–2061.

Tompa, P. (2011). Unstructural biology coming of age. Curr. Opin. Struct. Biol. *21*, 419–425.

Tompa, P., and Fuxreiter, M. (2008). Fuzzy complexes: polymorphism and structural disorder in protein-protein interactions. Trends Biochem. Sci. *33*, 2–8.

Tzeng, S.R., and Kalodimos, C.G. (2009). Dynamic activation of an allosteric regulatory protein. Nature *462*, 368–372.

Zhang, J., Yang, P.L., and Gray, N.S. (2009). Targeting cancer with small molecule kinase inhibitors. Nat. Rev. Cancer *9*, 28–39.

Update

Cancer Cell

Volume 30, Issue 1, 11 July 2016, Page 176–178

DOI: https://doi.org/10.1016/j.ccell.2016.06.015

Molecular Mechanism of SSR128129E, an Extracellularly Acting, Small-Molecule, Allosteric Inhibitor of FGF Receptor Signaling

Corentin Herbert, Ulrich Schieborr, Krishna Saxena, Jarek Juraszek, Frederik De Smet, Chantal Alcouffe, Marc Bianciotto, Giorgio Saladino, David Sibrac, Denis Kudlinzki, Sridhar Sreeramulu, Alan Brown, Patrice Rigon, Jean-Pascal Herault, Gilbert Lassalle, Tom L. Blundell, Frederic Rousseau, Ann Gils, Joost Schymkowitz, Peter Tompa, Jean-Marc Herbert, Peter Carmeliet, Francesco Luigi Gervasio,* Harald Schwalbe,* and Françoise Bono*
*Correspondence: flgervasio@cnio.es (F.L.G.), schwalbe@nmr.uni-frankfurt.de (H.S.), francoise.bono@sanofi-aventis.com (F.B.)
http://dx.doi.org/10.1016/j.ccell.2016.06.015

(Cancer Cell *23*, 489–501, April 15, 2013)

In Figure 2F, the authors failed to highlight clearly that there is a split in the western blot (all rows) between the "0" and "0.1" condition. Even though all samples were run in the same experiment on the same blot, the image was split to remove samples that were simultaneously analyzed but irrelevant for this study. In the corrected Figure 2F, the authors have now clearly separated both parts of the western blot.

In Figure 5B, the image of the western blot showing total FGFR2 for the HEK293-FGFR2^{Y328D} cell line was mistakenly replaced with the image of the western blot showing total FGFR2 for the HEK293-FGFR2^{WT} cell line from Figure 5A. In the corrected Figure 5B, the authors have included the correct image of the western blot showing total FGFR2 for the HEK293-FGFR2^{Y328D} cell line.

The corrected Figure 2 and Figure 5 are included below. The authors apologize for any confusion these mistakes may have caused the readers.

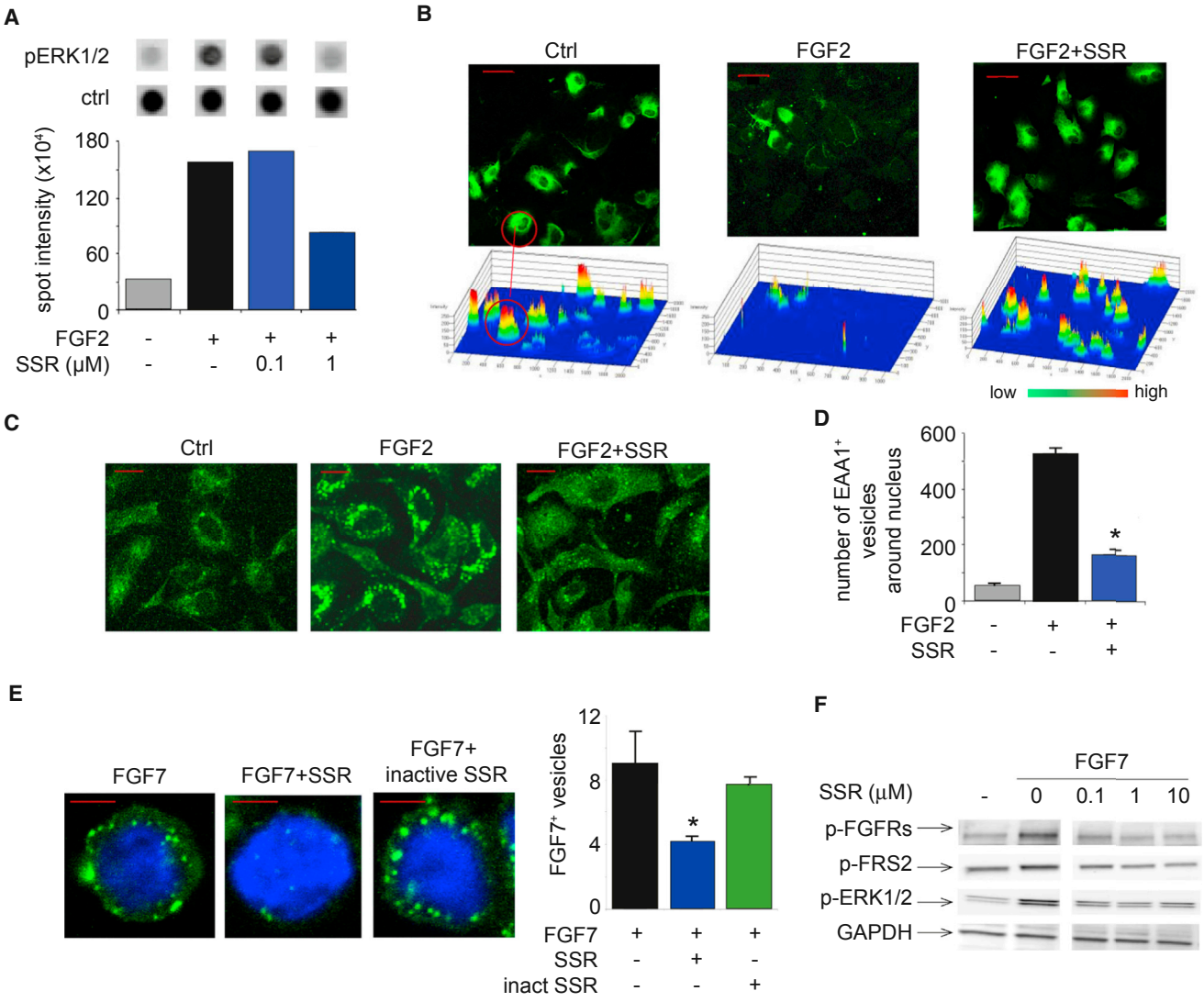

Figure 2. Effect of SSR on FGFR-Signaling and Endocytosis

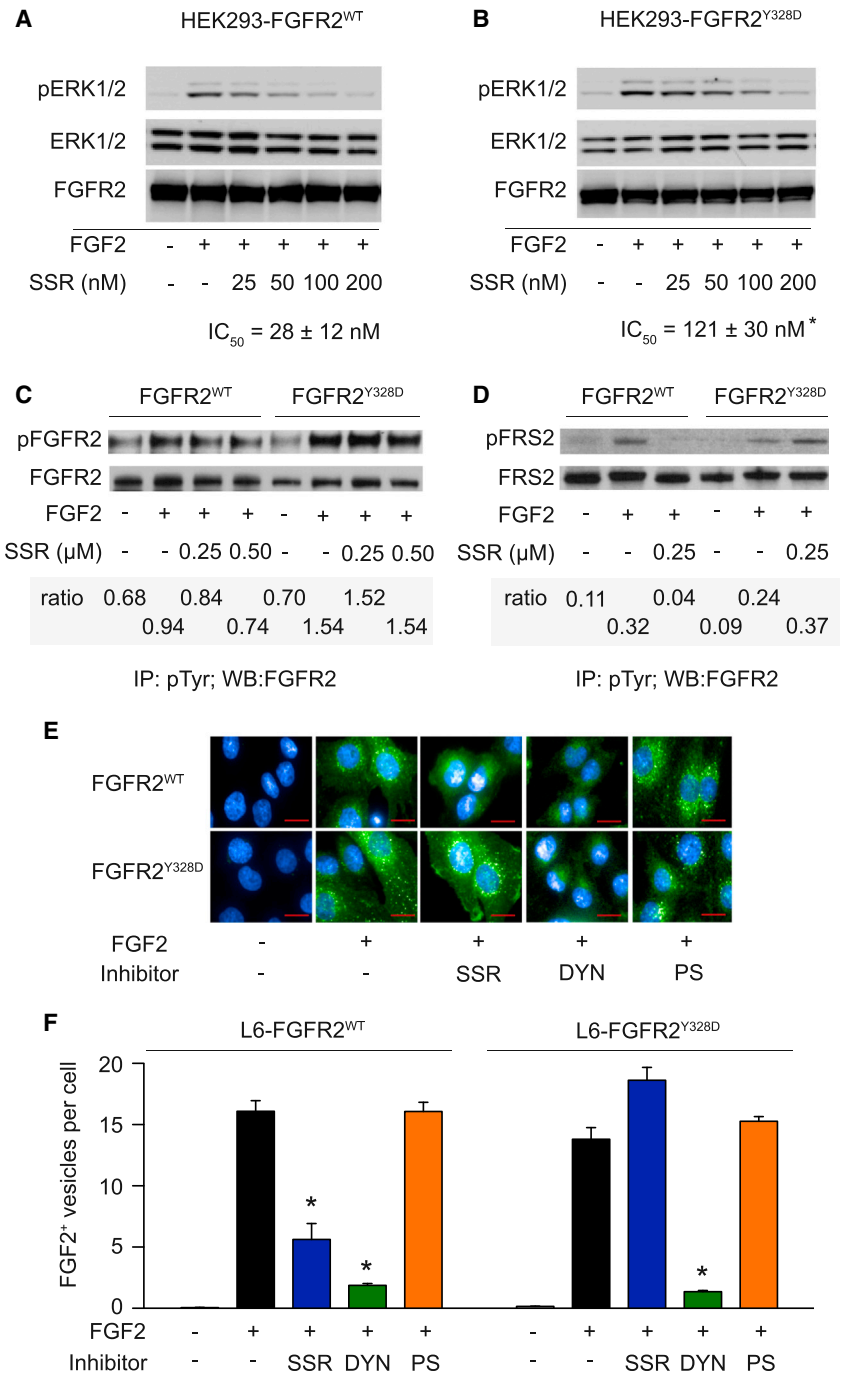

Figure 5. FGFR Signaling in FGFR2^{WT} and FGFR2^{Y328D} Cells